Bull. Mater. Sci. (2018) 41:27
https://doi.org/10.1007/s12034-017-1532-8

TiO_2 aerogel–metal organic framework nanocomposite: a new class of photoanode material for dye-sensitized solar cell applications

S ALWIN[1,2], V RAMASUBBU[1] and X SAHAYA SHAJAN[1,*]

[1]Center for Scientific and Applied Research, PSN College of Engineering and Technology, Melathediyoor, Tirunelveli 627152, India

[2]Department of Chemistry, Sri Shakthi Institute of Engineering and Technology, Coimbatore 641062, India

*Author for correspondence (shajan89@gmail.com)

MS received 9 November 2016; accepted 20 July 2017; published online 5 February 2018

Abstract. TiO_2 aerogel–metal organic framework (MOF) nanocomposite was synthesized using sol–gel method followed by subcritical drying technique and employed as a photoanode material in quasi-solid dye-sensitized solar cells (DSSCs). The nanocomposite material showed a BET surface area of 250 $m^2\ g^{-1}$ with an average pore size of 5 nm. Field emission scanning electron microscopic images revealed the continuous arrangement of pore-solid network structure. Energy-dispersive X-ray analysis shows the presence of MOF clusters on TiO_2 aerogel network. X-ray photoelectron spectroscopic analysis also supports the presence of MOF clusters in the aerogel network and indicates the presence of some oxygen vacancies in the nanocomposite material. The TiO_2 aerogel–MOF nanocomposite was used as photoanode in DSSC and an overall power conversion efficiency 2.34% along with a short-circuit current density 6.22 $mA\,cm^{-2}$ was achieved.

Keywords. Mesoporous materials; electron lifetime; band gap; network structure; oxygen vacancies; XPS.

1. Introduction

The emergence of dye-sensitized solar cells (DSSCs) challenged conventional photovoltaic devices because of its low cost, simple fabrication methods and reasonably good power conversion efficiency [1,2]. In DSSC, mesoporous titanium dioxide in association with a monolayer of dye molecules is responsible for absorption of photons and converts directly to electricity [3]. There are two major processes that mainly govern the power conversion efficiency of DSSC [4]. Firstly, absorption of photons from sunlight by mesoporous TiO_2 nanoparticles and Ru-based dyes, which directly affects the short-circuit current density. To improve photon absorption, physicochemical properties like morphology, size, surface area, band gap and surface chemistry of mesoporous TiO_2 were tailored [5,6]. The effect of TiO_2 particle size on DSSC performance was studied and reported that larger particles increases the amount of dye adsorption as well as power conversion efficiency [7,8]. Mesoporous TiO_2 with varying surface area was synthesized using different templates and achieved a superior DSSC performance [9]. High-surface area TiO_2 aerogels were obtained through microwave-assisted method and a maximum power conversion efficiency of 5.2% was attained in quasi-solid DSSCs [10]. Our recent reports show that plasma treatment of TiO_2 aerogel increases the specific surface area and hydrophilicity, which enhances the amount of dye adsorption, consequently, the DSSC performance [11,12]. It was reported that Au nanoparticle-decorated TiO_2 composite is enhancing the visible light absorption by decreasing the band gap [13]. Secondly, the recombination of electrons with oxidized dye molecules and redox electrolyte at the interface [14]. To suppress the recombination reactions occurring at interface, surface-modification methods, like $TiCl_4$, acid and oxygen-plasma treatment were adopted [15–17]. In addition, an insulating thin layer of Al_2O_3, SiO_2, ZrO_2 and HfO_2 was coated on nanocrystalline TiO_2 layer that acts as a blocking layer and hence, reduces recombination reactions [18,19].

Metal organic frameworks (MOF) are promising microporous materials, which find applications in energy storage and conversion due to its high surface area, variable pore sizes and low density [20]. Mg MOF with poly(ethylene glycol)methyl ether methacrylate, poly(ethylene glycol)diacrylate were prepared using UV-light-induced free radical process and used as quasi-solid gel electrolyte in DSSC [21]. A maximum power conversion efficiency of 4.8% was obtained with better durability. $Al_2(BDC)_3$ MOF was used as photoactive material along with TiO_2 and a short-circuit current density up to 36.2 $\mu A\ cm^{-2}$ was realized in DSSCs [22]. Recently, ZIF-8 was used as a shell layer on mesoporous TiO_2 and the energy barrier effect of ZIF-8 inhibits interfacial charge recombination. It was reported that when 2 nm thin layer of MOF coated on TiO_2, the open circuit potential of DSSC was increased, since the conduction band edge of ZIF-8 is slightly higher than that of TiO_2, which prevents the reverse electron flow to electrolyte [23]. Therefore, the MOF was used only as a separate blocking layer on TiO_2 for DSSC applications rather than as a composite material.

Composite aerogel is an emerging field increasing the design flexibility of the nanomaterials for optical, thermal and electronic applications. Rolison and group [24] developed a method for the preparation of composite aerogels in which the solid guest particles are introduced in the sol just before the gelation. In this method, the composite retains both the bulk and surface properties of each component [24]. Recently, TiO_2–MOF and SiO_2 aerogel–MOF composite materials were reported for different applications [25,26]. TiO_2 nanoparticle-coated ZnO nanorods were used as photoanode in DSSCs [27]. Binary metal oxide ZrO_2-TiO_2 composite electrode was employed as photoanode in DSSC [28]. In the present work, we report the sol–gel synthesis of TiO_2 aerogel–MOF nanocomposite and its usefulness as photoanode material in quasi-solid dye-sensitized solar cells (QSDSSC). This is a new class of nanocomposite material evaluated first time for DSSC applications. The power conversion efficiency, electron lifetime and charge collection efficiency of the DSSC with TiO_2-MOF nanocomposite material as photoanode is demonstrated.

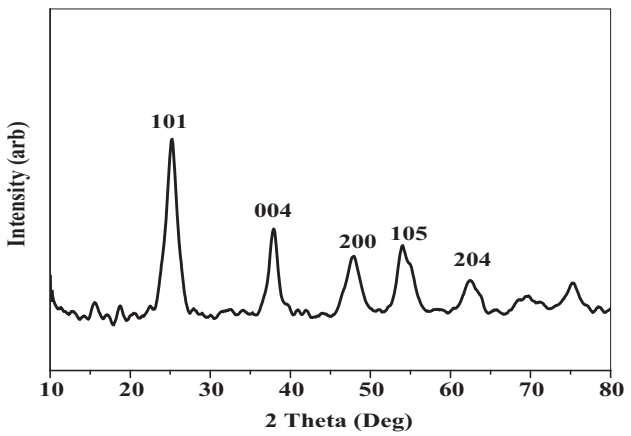

Figure 1. XRD pattern of TiO_2 aerogel–MOF nanocomposite.

2. Materials and methods

Titanium (IV) isopropoxide (TIP) was purchased from Sigma-Aldrich. Glacial acetic acid, ammonia solution (25%), 2-propanol and absolute ethanol (EtOH) were procured from Merck chemicals. Deionized water (18.2 MΩ) obtained from Millipore filtration system was used in experiments.

2.1 *Synthesis of TiO_2 aerogel–MOF composite*

TiO_2 aerogel–MOF nanocomposite was synthesized by the sol–gel method. Titanium isopropoxide (TIP) was stabilized using glacial acetic acid and subjected to hydrolysis with deionized water. The titania sol was stirred vigorously for 1 h. About 10 wt% of Zn–MOF with respect to TIP was added to the titania sol and the mixture was stirred for 2 h. The MOF [Zn(N-(4-pyridylmethyl)-L-valine · HCl)(Cl)]$(H_2O)_2$ was synthesized by the reported procedure [29]. Then, the pH of the sol was adjusted to 5 using 25% ammonia solution to initiate the condensation process. The gels were aged at 50°C for 24 h in deionized water. The wet gels were solvent exchanged repeatedly with 2-propanol at 50°C to remove water from the gel network. Finally, the gel network was dried at room temperature for 24 h.

2.2 *Characterization*

The powder XRD pattern of the TiO_2 aerogel–MOF composite was recorded using a PANalytical XPERT-PRO diffractometer with CuK α radiation (λ = 1.5406 Å). Brunauer–Emmet–Teller (BET) surface area measurements were performed by nitrogen adsorption at 77 K using a

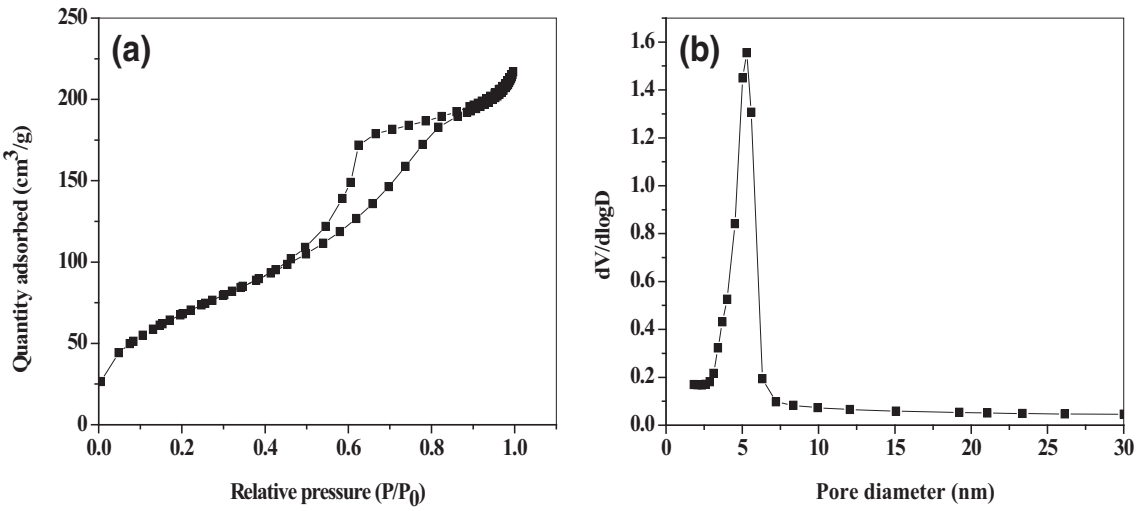

Figure 2. (**a**) BET adsorption–desorption isotherm and (**b**) BJH pore-size distribution analysis.

Micromeritics Tri-Star II 3020 analyzer. The pore size distribution was obtained from the desorption branches of isotherms using the Barrette–Joynere–Halenda (BJH) method. The morphology of nanocomposite was analysed using a field emission scanning electron microscope (FESEM-SUPRA55, CARL ZEISS). Transmission electron microscope (TEM) images were acquired on a JEOL/JEM 2100 TEM operated at 200 kV. The diffuse reflectance spectra of the composite were recorded using shimadzu-2600 UV–Vis spectrophotometer with an integrating sphere attachment. X-ray photoelectron spectra (XPS) was recorded using MgKα radiation (1253.5 eV) in a high-resolution spectrometer equipped with auto-charge neutralization (AXIS ULTRA, Kratos, UK). The photocurrent–voltage (*I–V*) characteristics and intensity-modulated photocurrent spectroscopy (IMPS)/intensity-modulated photovoltage spectroscopy (IMVS) were investigated using ZAHNER electrik IM6 electrochemical work station coupled with PP211 slave potentiostat to control the LED light source. The electron lifetime (τ_n) was determined from the IMVS spectra and the electron diffusion time (τ_d) was determined from the IMPS spectra by taking the minimum frequency of the semicircle [30].

2.3 *DSSC fabrication*

About 1 g of TiO_2 aerogel–MOF nanocomposite powder was dispersed in 4 ml of 2-propanol and spin-coated on the precleaned fluorinated tin oxide (FTO) substrates. The nanocomposite layer was dried at 120°C for 1 h under vacuum. After cooling to 80°C, the layer was soaked in 0.3 mM solutions of N-719 dye in ethanol for 24 h for sensitization. The counter electrode was prepared by spin-coating of 2 mM H_2PtCl_6 on FTO substrates and calcined at 350°C for 30 min. The quasi-solid gel electrolyte consists of poly(ethylene oxide)–poly(ethylene glycol)–NaI/I_2 and an ionic liquid 1-ethyl-3-methylimidazolium bis(trifluoromethylsulphonyl)imide in acetonitrile was prepared as per the reported procedure [31] and introduced on the photoanode. Finally, the DSSC was fabricated by sandwiching the quasi-solid polymer electrolyte between photoanode and the counter electrode.

3. Results and discussion

The XRD pattern for titania aerogel–MOF nanocomposite is presented in figure 1. The diffraction peaks observed at 2θ values 25.3°, 38°, 48°, 54° and 62.4° corresponds to 101, 004, 200, 105 and 204 planes of anatase phase of titania (JCPDS no: 21-1272), respectively. It indicates that the TiO_2 particles are preferentially crystallized in anatase phase. The broad diffraction peaks illustrate that the nanosized anatase crystals form the TiO_2 aerogel network. It is also supported by the crystallite size (16.5 nm) calculated using Debye–Scherrer equation from [101] plane. Also, it is observed that the Zn–MOF has not affected the anatase phase formation of TiO_2 crystals during synthesis.

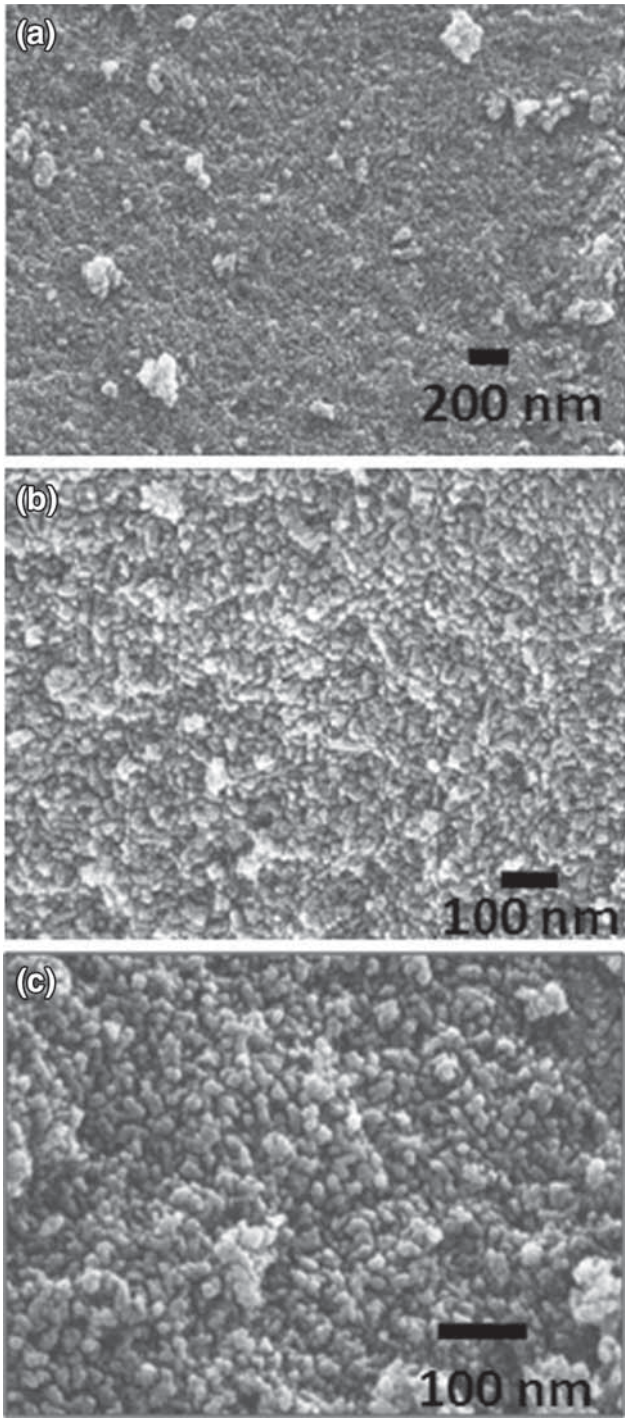

Figure 3. FESEM images of TiO_2 aerogel–MOF nanocomposite under (**a**) low and (**b**, **c**) high magnifications.

Figure 2a and b illustrates the BET isotherm and BJH pore-size distribution of the nanocomposite material. The BET isotherm shows Type-IV behaviour with an H2 hysteresis loop indicates a uniform pore structure in the mesoporous region. The increase in adsorption at low-pressure region indicates the presence of considerable amount of micropores due to MOF in the composite material. A hysteresis loop

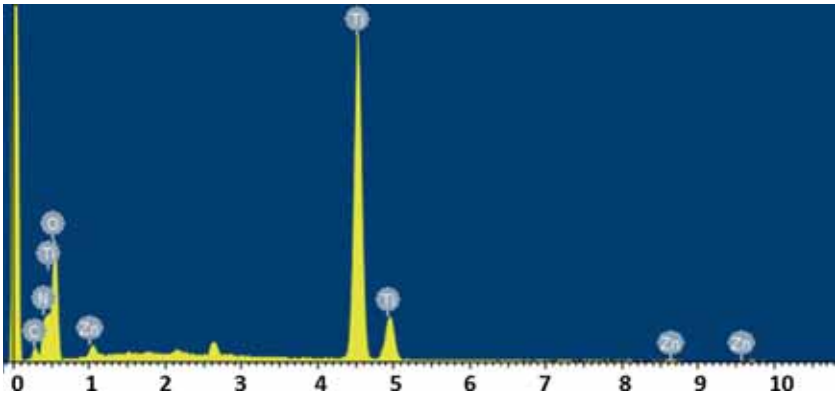

Figure 4. EDAX spectrum of TiO_2 aerogel–MOF nanocomposite.

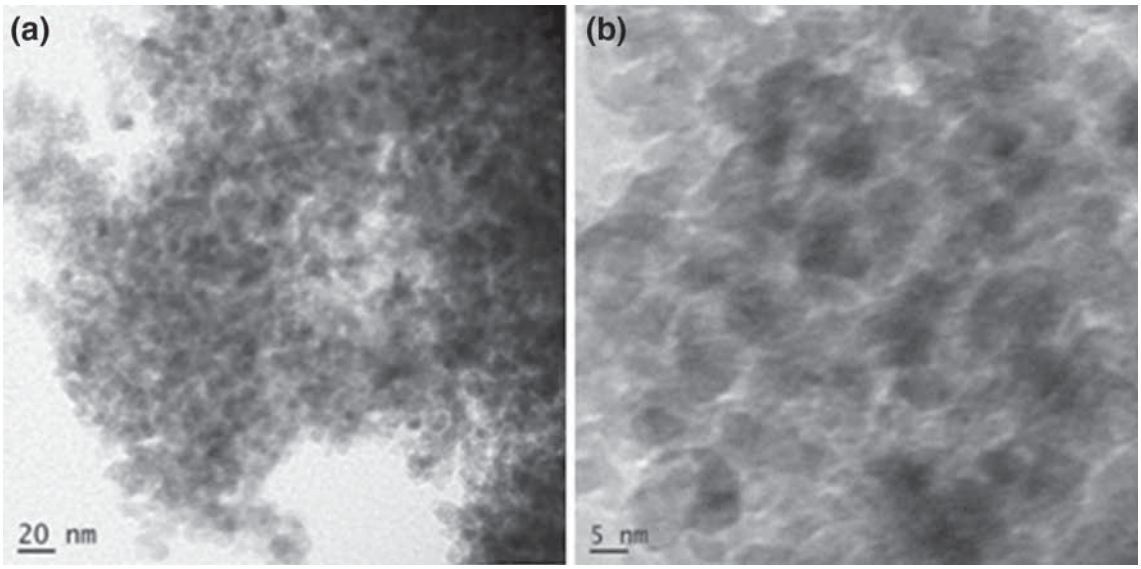

Figure 5. (**a**) TEM and (**b**) HRTEM images of TiO_2 aerogel–MOF nanocomposite.

at high-pressure region indicates the presence of mesopores and reveals that the structure consists of both mesopores and micropores. The BJH pore-size distribution confirms uniform pores with a narrow distribution curve compared to pristine TiO_2 aerogel (average pore size = 23 nm) and most of the pores are centred at 5 nm range. This suggests that the addition of microporous MOF to TiO_2 aerogel decreased the average pore size to 5 nm. The specific surface area of TiO_2 aerogel–MOF nanocomposite is 250 $m^2\ g^{-1}$, which is comparable with the surface area of TiO_2 aerogel (252 $m^2\ g^{-1}$). The addition of 10% MOF has not changed the surface area substantially. The MOF clusters may be attached to the surface of aerogel network and increase the surface area or left unchanged depending on the surface area of MOF. Conversely, the MOF may occupy the pores of aerogel network and reduce the surface area.

FESEM images of TiO_2 aerogel–MOF nanocomposite are presented in figure 3a and b. The FESEM image (figure 3a) shows uniformly arranged particles with an irregularly shaped aggregate on the surface. The particles are well interconnected with each other and form the continuous network structure. It is noteworthy to mention that the aerogel network structure is highly porous and the porous morphology is clearly visible from the FESEM image (figure 3b). It is also noted from the image that the microporous MOF clusters are attached to the surface of TiO_2 aerogel network. A continuous arrangement of the pore-solid network was evident from the FESEM image (figure 3c). Figure 4 describes the energy-dispersive X-ray analysis (EDAX) of the TiO_2 aerogel–MOF nanocomposite material. The EDAX spectrum indicates the presence of Zn, C and N in association with Ti and O, confirms the existence of MOF clusters in the nanocomposite material. In addition, it can be concluded that the MOF clusters were not completely leached out from the TiO_2 matrix during the solvent exchange performed in sol–gel synthesis. Figure 5a and b represents the TEM images of composite materials. A well-crystallized TiO_2 nanocrystals build the interconnected network structure of aerogel with nanopores is visible from

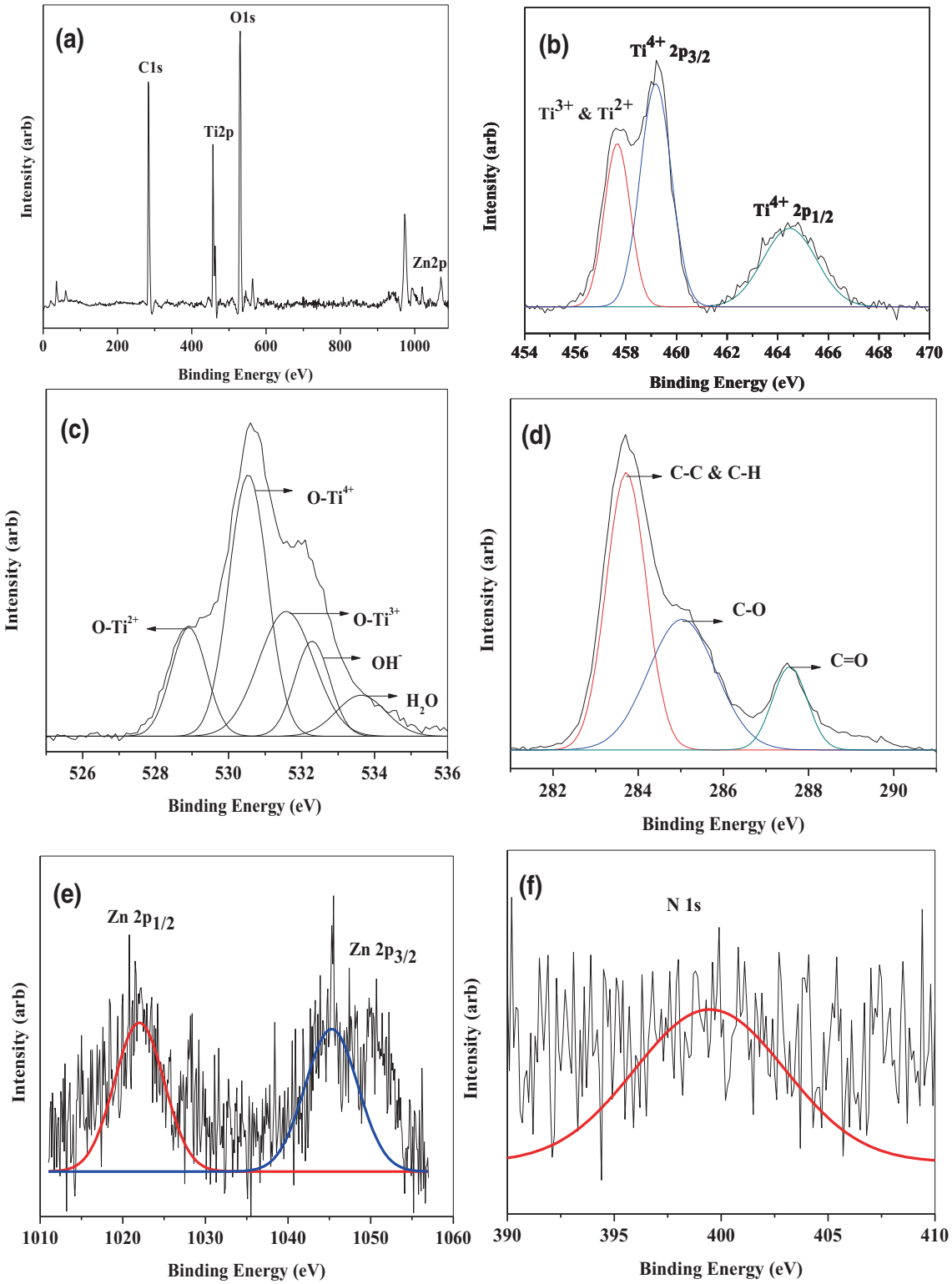

Figure 6. XPS analysis of TiO_2 aerogel–MOF nanocomposite, (**a**) survey spectra and HRXPS analysis of (**b**) Ti 2p, (**c**) O 1s, (**d**) C 1s, (**e**) Zn 2p and (**f**) N 1s.

the TEM images. These interconnected network structures offer good electron transport properties required for DSSC applications.

XPS was employed to study the chemical composition and electronic states of the TiO_2 aerogel–MOF nanocomposite. Figure 6 illustrates the survey spectra and high-resolution

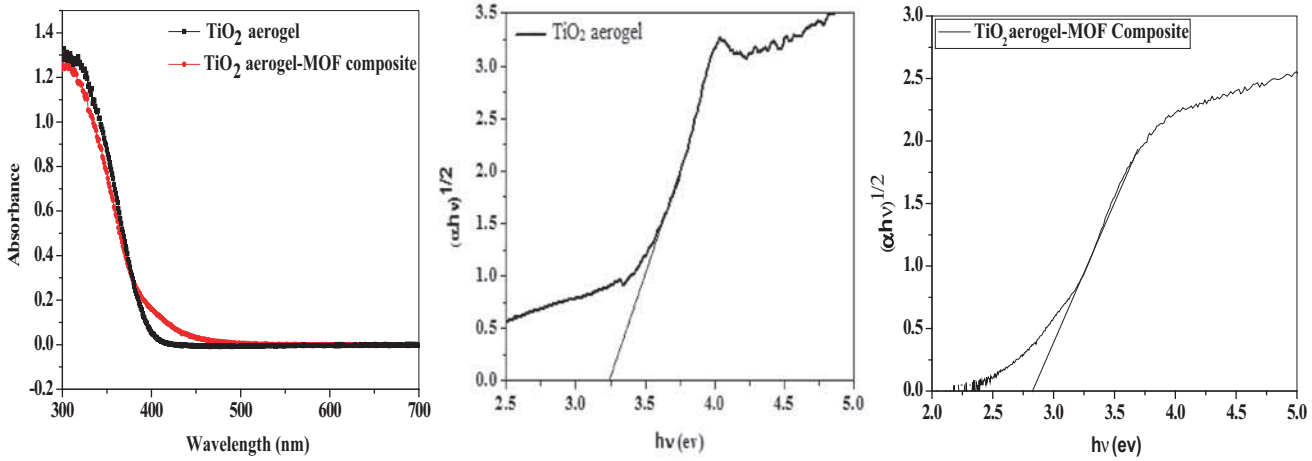

Figure 7. Diffuse reflectance spectra and Tauc's plot of TiO_2 aerogel–MOF composite.

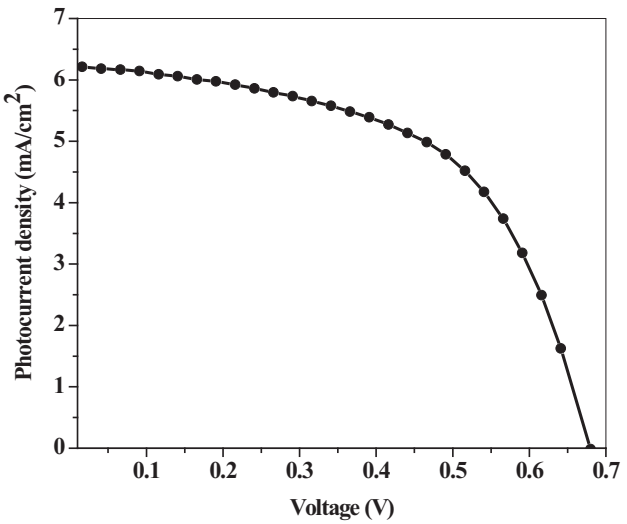

Figure 8. *I–V* characteristics of DSSC with TiO_2 aerogel–MOF nanocomposite as photoanodes.

XPS of individual elements. The survey spectra (figure 6a) mainly consists of Ti, O, C and a small amount of Zn indicates the formation of TiO_2 aerogel–MOF nanocomposite. Figure 6b represents the high-resolution XPS analysis of Ti2p. The deconvolution of Ti2p spectra shows two peaks at binding energies of 459.1 and 464.5 eV and demonstrates the core levels of $Ti^{4+}2p3/2$ and $Ti^{4+}2p1/2$. However, another peak observed at lower binding energy 457.6 eV indicates the sub-oxides (Ti^{3+}, Ti^{2+}) of TiO_2 [32]. Figure 6c illustrates the high-resolution O1s spectra, the deconvolution gives peaks at 530.5, 532.2 and 533.6 eV which correspond to oxide, surface hydroxyl groups (OH^-) and adsorbed H_2O molecules, respectively. The additional peaks detected at 531.5 and 528.9 eV are assigned to the sub-oxides of titania (Ti^{3+}, Ti^{2+}) as indicated by Ti2p spectrum [32]. This result clearly explains that oxygen vacancies or sub-oxides are introduced in the titania crystal during the formation of titania aerogel–MOF nanocomposite. The deconvolution peak at 283.7 eV of C1s spectra (figure 3d) is due to hydrocarbons (C−C, C−H) and another two peaks at 285 and 287.5 eV are due to C−O, C=O, respectively, indicating the presence of organic part of the MOF. Figure 6e and f illustrates the high-resolution spectra of Zn2p and N. The Zn2p spectrum shows two peaks at 1022.1 and 1045.2 eV, which are assigned to Zn^{2+} core levels of 2p3/2 and 2p1/2, respectively.

The absorption spectrum and the Tauc's plot of TiO_2 aerogel and nanocomposite is presented in figure 7. The absorption range is slightly shifted to longer wavelength for TiO_2 aerogel–MOF nanocomposite compared to pure TiO_2 aerogel. The band gap values obtained for pure TiO_2 aerogel and nanocomposite from the Tauc's plot are 3.2 and 2.8 eV, respectively. This indicates that the addition of MOF in TiO_2 aerogel structure may be introduced by some new electronic states between valence and conduction bands of TiO_2. This increases the photoactivity of the TiO_2 aerogel–MOF nanocomposite material in wider range of solar spectrum and is favourable to achieve better performance in DSSC.

Figure 8 represents the DSSC performance of TiO_2 aerogel and TiO_2 aerogel–MOF nanocomposite as photoanode materials and PEO−PEG−NaI/I_2/1-ethyl-3-methyl imidazolium bis(trifluoromethylsulphonyl) imide system as the quasi-solid polymer electrolyte. The photovoltaic and photoelectrical properties of the DSSCs are presented in table 1. The overall power conversion efficiency of 2.34% and a short-circuit current density (J_{sc}) of 6.22 mA cm^{-2} were achieved for DSSC with TiO_2 aerogel–MOF nanocomposite as photoanode. The reasonably good power conversion efficiency obtained using TiO_2 aerogel–MOF nanocomposite photoanode is attributed to the high-specific surface area of the nanocomposite material. The high-surface area of the photoanode material provides more space for adsorption of

Table 1. Photovoltaic and photoelectrical properties of DSSCs.

DSSC	V_{oc} (V)	J_{sc} (mA cm^{-2})	FF	η (%)	τ_n (ms)	τ_d (ms)	η_{cc}
TiO_2 aerogel	0.65	8.64	0.549	3.08	2.075	1.435	0.309
TiO_2 aerogel–MOF composite	0.68	6.22	0.553	2.34	1.384	1.002	0.276

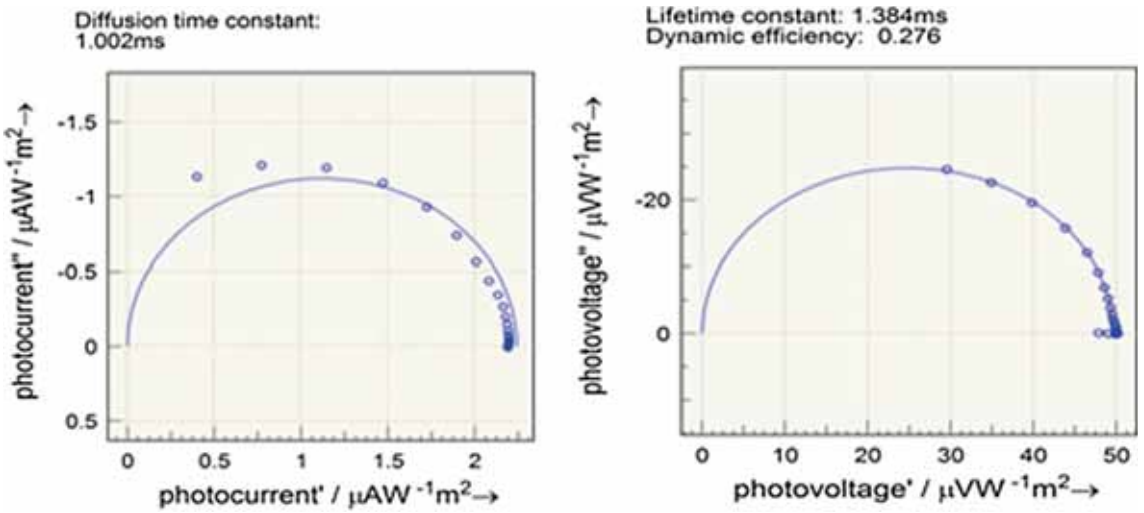

Figure 9. Intensity modulated photocurrent/photovoltage spectra of the TiO_2 aerogel–MOF nanocomposite photoanode-based DSSC.

dye molecules, which increases the photon absorption and hence, the short-circuit current density.

However, the power conversion efficiency is comparatively lower than that of P25-based DSSCs with PEO polymer electrolyte (3.84%) [33], which may be due to the following two reasons. Firstly, the smaller pores (5 nm) of nanocomposite will not allow the polymer electrolyte completely to penetrate the nanocomposite layer that will diminish the actual interface area near electrode/electrolyte interface due to the shrinkage of polymer, which limits the charge collection at the interface [34]. Secondly, the presence of more number of oxygen vacancies in the nanocomposite may be acting as electron trap sites, which increases the charge recombination of electrons. Other than this, the insulating nature of MOF may also have influenced the transport properties of nanocomposite material and decrease the power conversion efficiency. Therefore, the electron lifetime, diffusion time of the TiO_2 aerogel–MOF nanocomposite photoanode was determined from the IMVS/IMPS spectra presented in figure 9. The electron lifetime of TiO_2 aerogel–MOF naocomposite photoanode (1.384 ms) is found to be lower than P25-based DSSCs. Therefore, it is necessary to have the control over the density of electron trapping sites for realizing better performance in DSSC. Besides, the open circuit potential of the DSSC with nanocomposite photoanode is substantially higher due to the decrease in band gap by the introduction of new electronic levels in TiO_2 as determined by the Tauc's plot. Because, the open circuit potential of DSSC corresponds to the energy difference between the fermi level of TiO_2 and redox energy level of the electrolyte.

4. Conclusions

A new class of TiO_2 aerogel–MOF nanocomposite was synthesized by sol–gel method and employed it as a photoanode material in quasi-solid DSSCs. A maximum power conversion efficiency of 2.34% was achieved using TiO_2 aerogel–MOF nanocomposite as photoanode. The high surface area of the nanocomposite material enhanced the amount of dye adsorption as well as the short-circuit current density. XPS analysis revealed the presence of oxygen vacancies in nanocomposite material, which acts as the interfacial electron trap sites in DSSC. Therefore, the density of electron trapping sites and the insulating properties needs to be controlled by lowering the MOF in the composite material to realize a

better performance in DSSC with TiO_2 aerogel–MOF nanocomposite as photoanode.

Acknowledgements

Financial assistance from Science and Engineering Research Board (SERB), Department of Science and Technology (DST), Govt. of India, under the project sanction no. EMR/2014/000416 is gratefully acknowledged. We are grateful to CeNSE, IISc, Bangalore, for XPS analysis through Indian Nanoelectronics Users Progamme (INUP). We also thank Dr Rahul Banerjee, NCL, Pune, for his help rendered for the synthesis of MOF and Dr Bhaskar Bhattacharya, Dr Pramod K Singh, Department of Physics, Sharda University, Noida, for their help in polymer electrolyte preparation.

References

[1] Grätzel M 2003 *J. Photochem. Photobiol. C Photochem. Rev.* **4** 145
[2] Jena A, Mohanty S P, Kumar P, Johns N, Gondane V, Lekha P *et al* 2012 *Trans. Ind. Ceram. Soc.* **71** 1
[3] O'Regan B and Grätzel M 1991 *Nature* **353** 737
[4] Sero I M and Bisquert J 2010 *J. Phys. Chem. Lett.* **1** 3046
[5] Lee J K and Yang M 2011 *Mater. Sci. Eng.* **176** 1142
[6] Tu L, Pan H, Xie H, Yu A, Xu M, Chai M *et al* 2012 *Solid State Sci.* **14** 616
[7] Tammy P C, Zhang Q, Russo B, Fryxell G E and Cao G 2007 *J. Phys. Chem. C* **111** 6296
[8] Govindaraj R, Pandian M S, Ramasamy P and Mukhopadhyay S 2015 *Bull. Mater. Sci.* **38** 1
[9] Gajjela S R, Ananthanarayanan K, Yap C, Gratzel M and Balaya P 2010 *Energy Environ. Sci.* **3** 838
[10] Alwin S, Sahaya Shajan X, Karuppasamy K and Warrier K G K 2017 *Mater. Chem. Phys.* **196** 37
[11] Alwin S, Sahaya Shajan X, Menon R, Nabhiraj P Y, Warrier K G K and Mohan Rao G 2015 *Thin Solid Films* **595** 164
[12] Alwin S, Sahaya Shajan X, Ranjini Menon, Nabhiraj P Y and Ananthapadmanabhan P V 2017 *Mater. Res. Bull.* **86** 201
[13] Lim S P, Pandikumar A, Huang N M and Lim N H 2015 *RSC Adv.* **5** 44398
[14] Ondersma J W and Hamann T W 2013 *Coord. Chem. Rev.* **257** 1533
[15] Xin X, Scheiner M, Ye M and Lin Z 2011 *Langmuir* **27** 14594
[16] Kim B, Park S W, Kim J, Yoo K, Lee J, Lee M W *et al* 2013 *ACS Appl. Mater. Interface* **5** 5201
[17] Wu W, Shih T W, Chen P, Ting J M and Chen J M 2011 *J. Electrochem. Soc.* **158** K101
[18] Palomares E, Clifford J N, Haque S A, Lutz T and Durrant J 2003 *J. Am. Chem. Soc.* **125** 475
[19] Ramasamy P, Kang M S, Cha H J and Kim J 2013 *Mater. Res. Bull.* **48** 79
[20] Li S L and Xu Q 2013 *Energy Environ. Sci.* **6** 1656
[21] Bella F, Bongiovanni R, Senthil Kumar R, Anbu Kulandainathan M and Manuel Stephan A 2013 *J. Mater. Chem. A* **1** 9033
[22] Lopez H A, Dhakshinamoorthy A, Ferrer B, Atienzar P, Alvaro M and Garcia H 2011 *J. Phys. Chem. C* **115** 22200
[23] Li Y, Pang A, Wang C and Wei M 2011 *J. Mater. Chem.* **21** 17259
[24] Anderson M L, Stroud R M, Morris A, Merzbacher C and Rolison D R 2000 *Adv. Eng. Mater.* **8** 481
[25] Muller M, Zhang X, Wang Y and Fischer R A 2009 *Chem. Commun.* **1** 119
[26] Ulker Z, Erucar I, Keskin S and Erkey C 2013 *Microporous Mesoporous Mater.* **170** 352
[27] Manthina V, Baena J P, Liu G and Agrios A G 2012 *J. Phys. Chem. C* **116** 23864
[28] Asha R P and Nair B 2015 *Bull. Mater. Sci.* **38** 1129
[29] Sahoo S C, Kundu T and Banerjee R 2011 *J. Am. Chem. Soc.* **133** 17950
[30] DeSario P A, Pietron J J, Taffa D H, Compton R, Marschall R, Brintlinger T H *et al* 2015 *J. Phys. Chem. B* **119** 17529
[31] Singh P K, Bhattacharya B, Mehra R and Rhee H W 2011 *Curr. Appl. Phys.* **11** 616
[32] Liu G, Jaegermann W, He J, Sundstrom V and Sun L 2002 *J. Phys. Chem. B* **106** 5814
[33] Kang M S, Kim J H, Kim Y J, Park N G and Kang Y S 2005 *Chem. Commun.* **7** 889
[34] Lee J Y, Bhattacharya B, Kim Y, Jung Y and Park J K 2009 *Solid State Commun.* **149** 307